



Measurement of the running of the fine-structure constant

L3 Collaboration

M. Acciarri^z, P. Achard^s, O. Adriani^p, M. Aguilar-Benitez^y, J. Alcaraz^y,
G. Alemanni^v, J. Allaby^q, A. Aloisio^{ab}, M.G. Alviggi^{ab}, G. Ambrosi^s,
H. Anderhub^{au}, V.P. Andreev^{f,aj}, T. Angelescu^l, F. Anselmoⁱ, A. Arefiev^{aa},
T. Azemoon^c, T. Aziz^j, P. Bagnaia^{ai}, L. Baksay^{ap}, A. Balandras^d, R.C. Ball^c,
S. Banerjee^j, Sw. Banerjee^j, A. Barczyk^{au,as}, R. Barillère^q, L. Barone^{ai},
P. Bartalini^v, M. Basileⁱ, R. Battiston^{af}, A. Bay^v, F. Becattini^p, U. Beckerⁿ,
F. Behner^{au}, L. Bellucci^p, J. Berdugo^y, P. Bergesⁿ, B. Bertucci^{af}, B.L. Betev^{au},
S. Bhattacharya^j, M. Biasini^{af}, A. Biland^{au}, J.J. Blaising^d, S.C. Blyth^{ag},
G.J. Bobbink^b, A. Böhm^a, L. Boldizar^m, B. Borgia^{ai}, D. Bourilkov^{au},
M. Bourquin^s, S. Braccini^s, J.G. Branson^{al}, V. Brigljevic^{au}, F. Brochu^d,
A. Buffini^p, A. Buijs^{aq}, J.D. Burgerⁿ, W.J. Burger^{af}, A. Button^c, X.D. Caiⁿ,
M. Campanelli^{au}, M. Capellⁿ, G. Cara Romeoⁱ, G. Carlino^{ab}, A.M. Cartacci^p,
J. Casaus^y, G. Castellini^p, F. Cavallari^{ai}, N. Cavallo^{ab}, C. Cecchi^{af}, M. Cerrada^y,
F. Cesaroni^w, M. Chamizo^s, Y.H. Chang^{aw}, U.K. Chaturvedi^r, M. Chemarin^x,
A. Chen^{aw}, G. Chen^g, G.M. Chen^g, H.F. Chen^t, H.S. Chen^g, G. Chiefari^{ab},
L. Cifarelli^{ak}, F. Cindoloⁱ, C. Civinini^p, I. Clareⁿ, R. Clareⁿ, G. Coignet^d,
A.P. Colijn^b, N. Colino^y, S. Costantini^e, F. Cotorobai^l, B. Cozzoniⁱ,
B. de la Cruz^y, A. Csilling^m, S. Cucciarelli^{af}, T.S. Daiⁿ, J.A. van Dalen^{ad},
R. D'Alessandro^p, R. de Asmundis^{ab}, P. Déglon^s, A. Degré^d, K. Deiters^{as},
D. della Volpe^{ab}, P. Denes^{ah}, F. DeNotaristefani^{ai}, A. De Salvo^{au}, M. Diemoz^{ai},
D. van Dierendonck^b, F. Di Lodovico^{au}, C. Dionisi^{ai}, M. Dittmar^{au},
A. Dominguez^{al}, A. Doria^{ab}, M.T. Dova^{r,1}, D. Duchesneau^d, D. Dufournaud^d,
P. Duinker^b, I. Duran^{am}, H. El Mamouni^x, A. Engler^{ag}, F.J. Epplingⁿ, F.C. Erné^b,
P. Extermann^s, M. Fabre^{as}, R. Faccini^{ai}, M.A. Falagan^y, S. Falciano^{ai},
q, A. Favara^q, J. Fay^x, O. Fedin^{aj}, M. Felcini^{au}, T. Ferguson^{ag}, F. Ferroni^{ai},
H. Fesefeldt^a, E. Fiandrini^{af}, J.H. Field^s, F. Filthaut^q, P.H. Fisherⁿ, I. Fisk^{al},
G. Forconiⁿ, L. Fredj^s, K. Freudenreich^{au}, C. Furetta^z, Yu. Galaktionov^{aa,n},
S.N. Ganguli^j, P. Garcia-Abia^e, M. Gataullin^{ae}, S.S. Gau^k, S. Gentile^{ai,q},

N. Gheordanescu ^l, S. Giagu ^{ai}, Z.F. Gong ^t, G. Grenier ^x, O. Grimm ^{au},
 M.W. Gruenewald ^h, M. Guida ^{ak}, R. van Gulik ^b, V.K. Gupta ^{ah}, A. Gurtu ^j,
 L.J. Gutay ^{ar}, D. Haas ^e, A. Hasan ^{ac}, D. Hatzifotiadou ⁱ, T. Hebbeker ^h,
 A. Hervé ^q, P. Hidas ^m, J. Hirschfelder ^{ag}, A. Hirstius ^h, H. Hofer ^{au}, G. Holzner ^{au},
 H. Hoorani ^{ag}, S.R. Hou ^{aw}, I. Iashvili ^{at}, B.N. Jin ^g, L.W. Jones ^c, P. de Jong ^b,
 I. Josa-Mutuberría ^y, R.A. Khan ^r, M. Kaur ^{r,2}, M.N. Kienzle-Focacci ^s, D. Kim ^{ai},
 D.H. Kim ^{ao}, J.K. Kim ^{ao}, S.C. Kim ^{ao}, J. Kirkby ^q, D. Kiss ^m, W. Kittel ^{ad},
 A. Klimentov ^{n,aa}, A.C. König ^{ad}, A. Kopp ^{at}, V. Koutsenko ^{n,aa}, M. Kräber ^{au},
 R.W. Kraemer ^{ag}, W. Krenz ^a, A. Krüger ^{at}, A. Kunin ^{n,aa}, P. Ladron de Guevara ^y,
 I. Laktineh ^x, G. Landi ^p, K. Lassila-Perini ^{au}, M. Lebeau ^q, A. Lebedev ⁿ,
 P. Lebrun ^x, P. Lecomte ^{au}, P. Lecoq ^q, P. Le Coultre ^{au}, H.J. Lee ^h,
 J.M. Le Goff ^q, R. Leiste ^{at}, E. Leonardi ^{ai}, P. Levchenko ^{aj}, C. Li ^t, S. Likhoded ^{at},
 C.H. Lin ^{aw}, W.T. Lin ^{aw}, F.L. Linde ^b, L. Lista ^{ab}, Z.A. Liu ^g, W. Lohmann ^{at},
 E. Longo ^{ai}, Y.S. Lu ^g, K. Lübelmeyer ^a, C. Luci ^{q,ai}, D. Luckey ⁿ, L. Lugnier ^x,
 L. Luminari ^{ai}, W. Lustermann ^{au}, W.G. Ma ^t, M. Maity ^j, L. Malgeri ^q, A. Malinin ^q,
 C. Maña ^y, D. Mangeol ^{ad}, P. Marchesini ^{au}, G. Marian ^o, J.P. Martin ^x,
 F. Marzano ^{ai}, G.G.G. Massaro ^b, K. Mazumdar ^j, R.R. McNeil ^f, S. Mele ^q,
 L. Merola ^{ab}, M. Meschini ^p, W.J. Metzger ^{ad}, M. von der Mey ^a, A. Mihul ^l,
 H. Milcent ^q, G. Mirabelli ^{ai}, J. Mnich ^q, G.B. Mohanty ^j, P. Molnar ^h,
 B. Monteleoni ^{p,3}, T. Moulik ^j, G.S. Muanza ^x, F. Muheim ^s, A.J.M. Muijs ^b,
 M. Musy ^{ai}, M. Napolitano ^{ab}, F. Nessi-Tedaldi ^{au}, H. Newman ^{ac}, T. Niessen ^a,
 A. Nisati ^{ai}, H. Nowak ^{at}, Y.D. Oh ^{ao}, G. Organtini ^{ai}, A. Oulianov ^{aa}, C. Palomares ^y,
 D. Pandoulas ^a, S. Paoletti ^{ai,q}, P. Paolucci ^{ab}, R. Paramatti ^{ai}, H.K. Park ^{ag},
 I.H. Park ^{ao}, G. Pascale ^{ai}, G. Passaleva ^q, S. Patricelli ^{ab}, T. Paul ^k, M. Pauluzzi ^{af},
 C. Paus ^q, F. Pauss ^{au}, M. Pedace ^{ai}, S. Pensotti ^z, D. Perret-Gallix ^d, B. Petersen ^{ad},
 D. Piccolo ^{ab}, F. Pierella ⁱ, M. Pieri ^p, P.A. Piroué ^{ah}, E. Pistolesi ^z, V. Plyaskin ^{aa},
 M. Pohl ^s, V. Pojidaev ^{aa,p}, H. Postema ⁿ, J. Pothier ^q, N. Produit ^s, D.O. Prokofiev ^{ar},
 D. Prokofiev ^{aj}, J. Quartieri ^{ak}, G. Rahal-Callot ^{au,q}, M.A. Rahaman ^j, P. Raics ^o,
 N. Raja ^j, R. Ramelli ^{au}, P.G. Rancoita ^z, A. Raspereza ^{at}, G. Raven ^{al}, P. Razis ^{ac},
 D. Ren ^{au}, M. Rescigno ^{ai}, S. Reucroft ^k, T. van Rhee ^{aq}, S. Riemann ^{at}, K. Riles ^c,
 A. Robohm ^{au}, J. Rodin ^{ap}, B.P. Roe ^c, L. Romero ^y, A. Rosca ^h, S. Rosier-Lees ^d,
 J.A. Rubio ^q, D. Ruschmeier ^h, H. Rykaczewski ^{au}, S. Saremi ^f, S. Sarkar ^{ai},
 J. Salicio ^q, E. Sanchez ^q, M.P. Sanders ^{ad}, M.E. Sarakinos ^u, C. Schäfer ^q,
 V. Schegelsky ^{aj}, S. Schmidt-Kaerst ^a, D. Schmitz ^a, H. Schopper ^{av},
 D.J. Schotanus ^{ad}, G. Schwering ^a, C. Sciacca ^{ab}, D. Sciarrino ^s, A. Seganti ⁱ,
 L. Servoli ^{af}, S. Shevchenko ^{ae}, N. Shivarov ^{an}, V. Shoutko ^{aa}, E. Shumilov ^{aa},
 A. Shvorob ^{ae}, T. Siedenburger ^a, D. Son ^{ao}, B. Smith ^{ag}, P. Spillantini ^p, M. Steuer ⁿ,
 D.P. Stickland ^{ah}, A. Stone ^f, H. Stone ^{ah,3}, B. Stoyanov ^{an}, A. Straessner ^a,

K. Sudhakar ^j, G. Sultanov ^r, L.Z. Sun ^t, H. Suter ^{au}, J.D. Swain ^r, Z. Szillasi ^{ap,4},
 T. Sztaricskai ^{ap,4}, X.W. Tang ^g, L. Tauscher ^e, L. Taylor ^k, C. Timmermans ^{ad},
 Samuel C.C. Ting ⁿ, S.M. Ting ⁿ, S.C. Tonwar ^j, J. Tóth ^m, C. Tully ^q, K.L. Tung ^g,
 Y. Uchida ⁿ, J. Ulbricht ^{au}, E. Valente ^{ai}, G. Vesztergombi ^m, I. Vetlitsky ^{aa},
 D. Vicinanza ^{ak}, G. Viertel ^{au}, S. Villa ^k, M. Vivargent ^d, S. Vlachos ^e,
 I. Vodopianov ^{aj}, H. Vogel ^{ag}, H. Vogt ^{at}, I. Vorobiev ^{aa}, A.A. Vorobyov ^{aj},
 A. Vorvolakos ^{ac}, M. Wadhwa ^e, W. Wallraff ^a, M. Wang ⁿ, X.L. Wang ^t,
 Z.M. Wang ^t, A. Weber ^a, M. Weber ^a, P. Wienemann ^a, H. Wilkens ^{ad}, S.X. Wu ⁿ,
 S. Wynhoff ^q, L. Xia ^{ae}, Z.Z. Xu ^t, B.Z. Yang ^t, C.G. Yang ^g, H.J. Yang ^g,
 M. Yang ^g, J.B. Ye ^t, S.C. Yeh ^{ax}, An. Zalite ^{aj}, Yu. Zalite ^{aj}, Z.P. Zhang ^t,
 G.Y. Zhu ^g, R.Y. Zhu ^{ae}, A. Zichichi ^{i,q,r}, G. Zilizi ^{ap,4}, M. Zöller ^a

^a I. Physikalisches Institut, RWTH, D-52056 Aachen, Germany,
 and III. Physikalisches Institut, RWTH, D-52056 Aachen, Germany ⁵

^b National Institute for High Energy Physics, NIKHEF, and University of Amsterdam, NL-1009 DB Amsterdam, The Netherlands

^c University of Michigan, Ann Arbor, MI 48109, USA

^d Laboratoire d'Annecy-le-Vieux de Physique des Particules, LAPP, IN2P3-CNRS, BP 110, F-74941 Annecy-le-Vieux CEDEX, France

^e Institute of Physics, University of Basel, CH-4056 Basel, Switzerland

^f Louisiana State University, Baton Rouge, LA 70803, USA

^g Institute of High Energy Physics, IHEP, 100039 Beijing, China ⁶

^h Humboldt University, D-10099 Berlin, Germany ⁵

ⁱ University of Bologna and INFN-Sezione di Bologna, I-40126 Bologna, Italy

^j Tata Institute of Fundamental Research, Bombay 400 005, India

^k Northeastern University, Boston, MA 02115, USA

^l Institute of Atomic Physics and University of Bucharest, R-76900 Bucharest, Romania

^m Central Research Institute for Physics of the Hungarian Academy of Sciences, H-1525 Budapest 114, Hungary ⁷

ⁿ Massachusetts Institute of Technology, Cambridge, MA 02139, USA

^o KLTE-ATOMKI, H-4010 Debrecen, Hungary ⁴

^p INFN Sezione di Firenze and University of Florence, I-50125 Florence, Italy

^q European Laboratory for Particle Physics, CERN, CH-1211 Geneva 23, Switzerland

^r World Laboratory, FBLJA Project, CH-1211 Geneva 23, Switzerland

^s University of Geneva, CH-1211 Geneva 4, Switzerland

^t Chinese University of Science and Technology, USTC, Hefei, Anhui 230 029, China ⁶

^u SEFT, Research Institute for High Energy Physics, P.O. Box 9, SF-00014 Helsinki, Finland

^v University of Lausanne, CH-1015 Lausanne, Switzerland

^w INFN-Sezione di Lecce and Università Degli Studi di Lecce, I-73100 Lecce, Italy

^x Institut de Physique Nucléaire de Lyon, IN2P3-CNRS, Université Claude Bernard, F-69622 Villeurbanne, France

^y Centro de Investigaciones Energéticas, Medioambientales y Tecnológicas, CIEMAT, E-28040 Madrid, Spain ⁸

^z INFN-Sezione di Milano, I-20133 Milan, Italy

^{aa} Institute of Theoretical and Experimental Physics, ITEP, Moscow, Russia

^{ab} INFN-Sezione di Napoli and University of Naples, I-80125 Naples, Italy

^{ac} Department of Natural Sciences, University of Cyprus, Nicosia, Cyprus

^{ad} University of Nijmegen and NIKHEF, NL-6525 ED Nijmegen, The Netherlands

^{ae} California Institute of Technology, Pasadena, CA 91125, USA

^{af} INFN-Sezione di Perugia and Università Degli Studi di Perugia, I-06100 Perugia, Italy

^{ag} Carnegie Mellon University, Pittsburgh, PA 15213, USA

^{ah} Princeton University, Princeton, NJ 08544, USA

^{ai} INFN-Sezione di Roma and University of Rome, "La Sapienza", I-00185 Rome, Italy

^{aj} Nuclear Physics Institute, St. Petersburg, Russia

^{ak} University and INFN, Salerno, I-84100 Salerno, Italy

^{al} University of California, San Diego, CA 92093, USA

^{am} Dept. de Física de Partículas Elementales, Univ. de Santiago, E-15706 Santiago de Compostela, Spain

^{an} Bulgarian Academy of Sciences, Central Lab. of Mechatronics and Instrumentation, BU-1113 Sofia, Bulgaria

^{ao} Center for High Energy Physics, Adv. Inst. of Sciences and Technology, 305-701 Taejon, South Korea^{ap} University of Alabama, Tuscaloosa, AL 35486, USA^{aq} Utrecht University and NIKHEF, NL-3584 CB Utrecht, The Netherlands^{ar} Purdue University, West Lafayette, IN 47907, USA^{as} Paul Scherrer Institut, PSI, CH-5232 Villigen, Switzerland^{at} DESY, D-15738 Zeuthen, Germany^{au} Eidgenössische Technische Hochschule, ETH Zürich, CH-8093 Zürich, Switzerland^{av} University of Hamburg, D-22761 Hamburg, Germany^{aw} National Central University, Chung-Li, Taiwan, ROC^{ax} Department of Physics, National Tsing Hua University, Taiwan, ROC

Received 7 January 2000; accepted 25 January 2000

Editor: K. Winter

Abstract

Small-angle Bhabha scattering data recorded at the Z resonance and large-angle Bhabha scattering data recorded at $\sqrt{s} = 189 \text{ GeV}$ by the L3 detector at LEP are used to measure the running of the effective fine-structure constant for spacelike momentum transfers. The results are

$$\alpha^{-1}(-2.1 \text{ GeV}^2) - \alpha^{-1}(-6.25 \text{ GeV}^2) = 0.78 \pm 0.26$$

$$\alpha^{-1}(-12.25 \text{ GeV}^2) - \alpha^{-1}(-3434 \text{ GeV}^2) = 3.80 \pm 1.29,$$

in agreement with theoretical predictions. © 2000 Published by Elsevier Science B.V. All rights reserved.

1. Introduction

At zero momentum transfer, the QED [1] fine structure constant $\alpha(0)$ is very accurately known from the measurement of the anomalous magnetic moment of the electron and from solid-state physics measurements [2]:

$$\alpha^{-1}(0) = 137.035\,999\,76(50).$$

In QED, vacuum polarization corrections to processes involving the exchange of virtual photons

result in a Q^2 dependence, or running, of the *effective* fine-structure constant, $\alpha(Q^2)$. This Q^2 dependence is usually parametrised [3] as

$$\alpha(Q^2) = \frac{\alpha(0)}{1 - \Delta\alpha(Q^2)}. \quad (1)$$

Whereas the leptonic contributions to $\Delta\alpha(Q^2)$ can be accurately calculated, due to non-perturbative QCD effects the vacuum polarization contributions from quark loops cannot be calculated exactly. Therefore, dispersion integral techniques [4–6] are used to estimate these contributions from the measured cross sections for the process $e^+e^- \rightarrow \text{hadrons}$ at low centre-of-mass energies, yielding at $Q^2 = m_Z^2$: $\alpha^{-1}(m_Z^2) = 128.886 \pm 0.090$. Similar evaluations have been made in Ref. [7,8] and, under additional theoretical assumptions, in Refs. [9–13].

Processes involving photon exchange at non-zero momentum transfer Q^2 yield amplitudes proportional to $\alpha(Q^2)$. At e^+e^- colliders this implies that the measurement of the relative rates of processes involving different Q^2 values gives access to the running of $\alpha(Q^2)$ between those Q^2 values. This

¹ Also supported by CONICET and Universidad Nacional de La Plata, CC 67, 1900 La Plata, Argentina.

² Also supported by Panjab University, Chandigarh-160014, India.

³ Deceased.

⁴ Also supported by the Hungarian OTKA fund under contract numbers T22238 and T026178.

⁵ Supported by the German Bundesministerium für Bildung, Wissenschaft, Forschung und Technologie.

⁶ Supported by the National Natural Science Foundation of China.

⁷ Supported by the Hungarian OTKA fund under contract numbers T019181, F023259 and T024011.

⁸ Supported also by the Comisión Interministerial de Ciencia y Tecnología.

was first exploited by the TOPAZ Collaboration [14], which derived a value of the fine structure constant at a scale of $Q^2 = 3338 \text{ GeV}^2$ from the ratio of the muon pair annihilation cross section to the two-photon-induced muon pair cross section.

In regions where Bhabha scattering is dominated by t -channel photon exchange, this process allows the study of $\alpha(Q^2)$ in the spacelike region, $Q^2 = t = -s(1 - \cos\theta)/2 < 0$, where θ is the angle of the outgoing e^- with respect to the e^- beam direction. The VENUS Collaboration has recently interpreted large-angle Bhabha scattering measurements in terms of the evolution of $\alpha(Q^2)$ in the range $100 \text{ GeV}^2 < -Q^2 < 2916 \text{ GeV}^2$ [15].

This article interprets measurements of Bhabha scattering by the L3 experiment at LEP in terms of the evolution of $\alpha(Q^2)$, using two complementary measurements: first, an analysis of the small-angle Bhabha scattering data in the polar angular range $32 \text{ mrad} < \theta < 54 \text{ mrad}$, collected at centre-of-mass energies around the Z mass and used for the high-precision luminosity measurement in the years 1993–1995; second, the measurement of the Bhabha scattering cross section in the polar angular range $20^\circ < \theta < 36^\circ$ performed at $\sqrt{s} = 188.7 \text{ GeV}$ in 1998. They are used to study the running of $\alpha(Q^2)$ in the range $2.1 \text{ GeV}^2 < -Q^2 < 6.25 \text{ GeV}^2$ and $12.25 \text{ GeV}^2 < -Q^2 < 3434 \text{ GeV}^2$, respectively.

2. Small-angle Bhabha scattering

2.1. Data analysis

The analysis of the small-angle Bhabha scattering data follows closely that of the luminosity measurement [16], and makes use of the same detectors:

- two small-angle calorimeters consisting of BGO crystals, providing a precise energy measurement for electromagnetic showers. The highest-energy cluster reconstructed in each calorimeter is retained for analysis. The energy of one cluster must exceed $0.8 E_{\text{beam}}$; the energy of the cluster in the other calorimeter must be greater than $0.4 E_{\text{beam}}$. To avoid edge effects their reconstructed polar angles must be well contained in the calorimeter, $28 \text{ mrad} < \theta < 65 \text{ mrad}$;

- a silicon strip detector, consisting of two layers of r -measuring strips and one layer of ϕ -measuring strips, installed in front of each BGO calorimeter. This detector allows a precise definition of the fiducial volume. The coordinates of the cluster reconstructed in the calorimeter are projected onto each r -measuring silicon detector plane in turn, and a matching window (5 mm for r -measuring strips and 2.5° for ϕ -measuring strips) is used to search for corresponding hit strips. If found, their coordinates are used. Otherwise the BGO coordinates are retained.

Angular cuts are applied on the coordinate measurements for each r -measuring plane in turn. The fiducial volume is the same as that used for the luminosity measurement ($32 \text{ mrad} < \theta < 54 \text{ mrad}$), divided into four polar angular bins, with boundaries at 32, 35, 40, 46, and 54 mrad. For each event, each of the four coordinate measurements (two on each side) is entered in the corresponding angular bin with a weight of 0.25.

The silicon coordinate reconstruction is sensitive to malfunctioning silicon strips. Therefore, only those data are used for which the silicon detector was fully functional, resulting in a sample of $6.7 \cdot 10^6$ Bhabha events corresponding to an integrated luminosity of 98.8 pb. In addition, the polar angular bins are chosen to have boundaries sufficiently far away from malfunctioning strips (8 in 1993, 9 in 1994, and 11 in 1995) and from the edges of the flare in the beam pipe (42.5 and 50 mrad) on the outgoing e^- side. The data are grouped into 7 sets, according to the three years and the different centre-of-mass energies.

Detector effects are corrected for, bin by bin, using a sample of $2.6 \cdot 10^6$ fully simulated [17] and reconstructed BHLUMI [18] Monte Carlo events. The correction factors differ from 1 by at most 0.4% and have statistical uncertainties of about $4 \cdot 10^{-4}$.

The data are compared with predictions from the BHLUMI Monte Carlo program. This program is modified to allow the running of $\alpha(Q^2)$ in the spacelike region to be different from the nominal one of Ref. [4]. The running in the timelike region is left unchanged. This is relevant for the interference term between the dominant t -channel photon-exchange and the s -channel Z -exchange diagrams, which contributes up to 0.15% to the Bhabha cross section in the luminosity monitor fiducial volume at centre-of-

mass energies around the Z resonance. The predictions are calculated for each data set separately.

Since the small-angle Bhabha scattering data are used for the absolute normalisation of all processes, only the shape of the polar angular distribution can be used in this study. Therefore, the compatibility of the data with any given parametrisation, p , of the running of $\alpha(Q^2)$ is evaluated in terms of a likelihood formula according to multinomial statistics:

$$-\ln \mathcal{L} = - \sum_i \ln P(n_{1,i}, \dots, n_{4,i}; f_{1,i}^p, \dots, f_{4,i}^p), \quad (2)$$

where

$$f_{j,i}(p) = \int_{\theta_{j,i,\min}}^{\theta_{j,i,\max}} \frac{d\sigma^p}{d\theta} d\theta \bigg/ \int_{\theta_{\min}}^{\theta_{\max}} \frac{d\sigma^p}{d\theta} d\theta$$

is the fractional cross section predicted in bin j ($= 1 \dots 4$) for data set i ($= 1 \dots 7$) for parametrisation p , $n_{j,i}$ is the observed event weight in each angular bin, and P is the multinomial probability distribution.

2.2. Results

The data are first compared with two hypotheses: the theoretical prediction [4] (referred to as ‘normal running’) and the prediction for the case of no running of $\alpha(Q^2)$ between Q^2 and the lowest scale accessible in the analysis, $Q_0^2 = -2.1 \text{ GeV}^2$. Fig. 1 shows, for the 1994 data which have the highest statistics, the ratio of the measured and expected fractional event weights for the two hypotheses. The likelihood difference between the two hypotheses is $-(\ln \mathcal{L}(\text{no running}) - \ln \mathcal{L}(\text{normal running})) = 10.24$ for the complete data set, excluding the hypothesis of no running by 4.5σ .

The data are then compared with a parametrisation in which a term, linear in Q^2 and with a slope, S , to be fitted, is added to the normal running. The Q^2 dependence of Eq. (1) then becomes

$$\alpha(Q^2) = \frac{\alpha(0)}{1 - \Delta\alpha(Q^2) - S \cdot (Q^2 - Q_0^2)}, \quad (3)$$

with Q_0^2 as given above. The fit yields the result $S = (-3.6 \pm 2.7) \cdot 10^{-4} \text{ GeV}^{-2}$, where the error is statistical only.

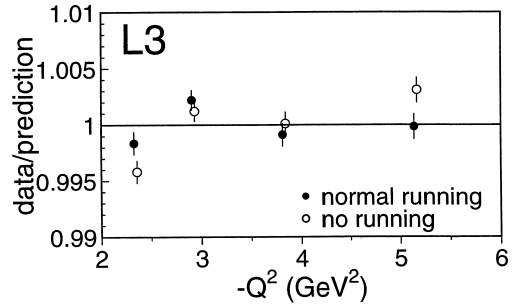


Fig. 1. Ratio of the measured and expected fractional event weights in each polar angular bin for the standard theoretical predictions (solid circles) and the assumption of no running (open circles), for the data collected in 1994.

The following sources of systematic uncertainties on S have been studied:

- Statistical uncertainties on the detector correction factors: their effect is studied by generating a large number of random number sequences in which each correction factor is changed according to a Gaussian distribution having a width equal to its statistical uncertainty. Since the same Monte Carlo sample is always used for the corrections, the changes in the correction factors are assumed to be fully correlated between the same bins of different data sets. Each time the corrections are changed, and the spread in the fitted values of S is found to be $1.5 \cdot 10^{-4} \text{ GeV}^{-2}$;
- Statistical uncertainties on the theoretical predictions: their effect is studied in the same way. In this case, the statistical uncertainties on the cross sections are assumed to be fully correlated between different choices of the parametrisation of $\alpha(Q^2)$, but to be uncorrelated between different data sets. This yields an uncertainty of $0.5 \cdot 10^{-4} \text{ GeV}^{-2}$.
- The size of the matching window used for the coordinate reconstruction: this is studied by changing it to 4 mm and 2° for the r - and ϕ -measuring strips, respectively, and the difference in the fit result ($0.8 \cdot 10^{-4} \text{ GeV}^{-2}$) is assigned as a systematic uncertainty.
- The consistency between the results obtained using the individual r -measuring silicon layers: instead of combining the results from the four r -measuring layers, the analysis can also be performed for each side or layer separately. The

fitted values of S are $-6.7 \cdot 10^{-4}$ using the layers on the outgoing e^+ ($-z$) side, and $-0.5 \cdot 10^{-4}$ using the layers on the outgoing e^- ($+z$) side. The results obtained using each of the two layers on either side are in excellent agreement with each other.

From the ratio of the (corrected) fractions in each bin for the $-z$ and $+z$ sides, the difference is seen to be due to a rather poor overall agreement between the observed fractions for the two sides. The cause for this poor agreement is an incomplete simulation of the beampipe material traversed at small angles by the e^\pm before entering the silicon detector. The uncertainty assigned to this source is half the difference between the results for the two sides, $3.1 \cdot 10^{-4}$. This dominates the total measurement uncertainty.

As a cross-check on the material effects, the last two bins are merged into a single bin which covers the complete region of increased material in the flare of the beam pipe. An alternative is to take out from the analysis the first bin, which represents the most material for the layers on the other side. In both cases the results are stable within the systematic uncertainty assigned.

Finally, the effect of the choice of polar angular bins is studied by performing the fits for several choices of binning. Variations of the size of the systematic uncertainty assigned are found, which are almost entirely due to variations observed on the $+z$ side. Their cause is the same as that of the poor overall agreement, and no additional systematic uncertainty is assigned.

- The uncertainty on the vertex position: this affects the two sides in opposite ways. Its effect has been estimated by artificially moving the vertex position, and is found to be negligible.

The largest contribution (0.04%) to the theoretical systematic uncertainty on the luminosity measurement at centre-of-mass energies around the Z resonance [19] comes from the theoretical uncertainty on the value of $\alpha(Q^2)$ in the small-angle Bhabha scattering region, and hence should not be considered in this analysis. Theoretical uncertainties on other contributions can affect the angular dependence only slightly. For example, the uncertainty due to missing $\mathcal{O}(\alpha^3 L^3)$ (where L represents the ‘large logarithm’ $\ln(|t|/m_e)$) contributions to the uncertainty on S is

estimated to be about $4 \cdot 10^{-6}$, i.e. negligible compared to the experimental systematics.

The final result of the measurement of S is thus

$$S = (-3.6 \pm 2.7(\text{stat.}) \pm 3.5(\text{syst.})) \cdot 10^{-4} \text{ GeV}^{-2}. \quad (4)$$

3. Large-angle Bhabha scattering

3.1. Data Analysis

The subdetectors used for the measurement of large-angle Bhabha scattering are the BGO electromagnetic calorimeter and the central tracker, described in detail in Ref. [20]. The data were collected in 1998 at $\sqrt{s} = 188.7 \text{ GeV}$ and correspond to an integrated luminosity of 175.9 pb . Electrons are identified as energy deposits of at least 0.5 GeV in the calorimeter, with an electromagnetic transverse shower shape, and at least six associated track hits within a three degree azimuthal angular range. At least one electron must be observed within the fiducial volume $20^\circ < \theta < 36^\circ$, and one within $144^\circ < \theta < 160^\circ$. At most six electromagnetic clusters are admitted in the electromagnetic calorimeter. The highest-energy electron must have an energy exceeding $0.5 E_{\text{beam}}$. In this angular range, t -channel photon exchange gives the dominant contribution to the cross section, with s - t interference and s -channel exchange contributing only -7% and 0.3% , respectively.

The signal efficiency is estimated using $2.5 \cdot 10^6$ fully simulated and reconstructed BHWIDE [21] Monte Carlo events generated in the angular range $5^\circ < \theta < 175^\circ$. The background, consisting mainly of $e^+e^- \rightarrow \tau^+\tau^-(\gamma)$ events, is small, 0.12% , and its uncertainty has a negligible effect on the cross section measurement.

Given the large Q^2 range covered by this analysis, the parametrisation of Eq. (3) is not appropriate. Deviations from the normal running of $\alpha(Q^2)$ are parametrised, for any Q^2 , using the following modification of Eq. (1):

$$\alpha(Q^2) = \frac{\alpha(0)}{1 - C \cdot \Delta\alpha(Q^2)}, \quad (5)$$

where $\Delta\alpha(Q^2)$ is calculated according to Ref. [4]. The evolution of $\alpha(Q^2)$ is then determined from

the ratio of measured to predicted cross sections, $\sigma_{\text{meas}}/\sigma_{\text{pred}}(C)$, where $\sigma_{\text{pred}}(C)$ is the predicted cross section for a given value of C . Since Eq. (5) also modifies the value of $\alpha(Q^2)$ in the Q^2 range used for the luminosity measurement, also the measured luminosity and hence the measured cross section is changed for $C \neq 1$. This is accounted for by the use of the ratio

$$R(C) = \frac{\sigma_{\text{meas}}}{\sigma_{\text{pred}}(C)} \cdot \frac{\sigma_{\text{lumi}}(C)}{\sigma_{\text{lumi}}(C=1)}, \quad (6)$$

where $\sigma_{\text{lumi}}(C)$ is the small-angle Bhabha scattering cross section in the fiducial volume used for the luminosity measurement. C is then determined by equating $R(C) = 1$. The cross section predictions are obtained using the BHWIDE and BHLUMI Monte Carlo programs for the large-angle and small-angle Bhabha scattering processes, respectively, modified to parametrise the evolution of $\alpha(Q^2)$ according to Eq. (5).

3.2. Results

The number of selected events is 23940. The selection efficiency is estimated to be $(93.38 \pm 0.08)\%$, where the error is due to limited Monte Carlo statistics. The measured cross section is $\sigma_{\text{meas}} = 145.6 \pm 0.9$ pb.

Systematic uncertainties on the cross section measurement are due to:

- The description of the energy response: Fig. 2 shows the energy of the highest-energy electron, normalised to E_{beam} . The low-energy tail of the distribution is not very well described by the Monte Carlo simulation. Its effect on the selection efficiency is estimated by adjusting the Monte Carlo distribution to obtain a better agreement, and is found to be negligible.
- The definition of the fiducial volume: this is estimated by varying the angular cuts and results in a 0.4% uncertainty.
- The cut on the number of track hits: a comparison between data and Monte Carlo events has been used to adjust the Monte Carlo description of the single-hit efficiency of the inner tracker wires. Varying the cut on the number of hits changes the efficiency by 0.3%.

Summing the individual contributions in quadrature, a total systematic uncertainty of 0.5% is ob-

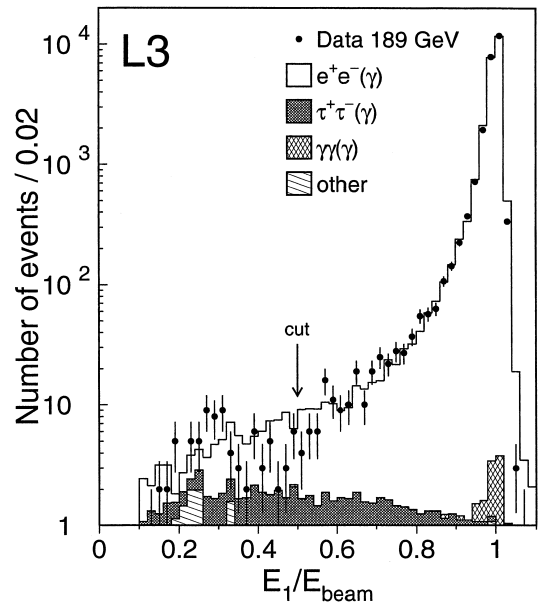


Fig. 2. Distribution of the highest electron energy normalised to the beam energy. The arrow shows the position of the applied cut.

tained. The result of the cross section measurement is thus

$$\sigma_{\text{meas}} = 145.6 \pm 0.9(\text{stat.}) \pm 0.8(\text{syst.}) \text{ pb.} \quad (7)$$

The measured cross section agrees well with the theoretical prediction of $\sigma_{\text{pred}}(C=1) = 145.9$ pb. Using Eq. (6) and assuming a theoretical uncertainty on $\sigma_{\text{pred}}(C=1)$ of 1.5% [22], the value of C obtained is $C = 0.97 \pm 0.12(\text{stat.}) \pm 0.10(\text{syst.}) \pm 0.29(\text{theory})$.

4. Interpretation of results

The results can be interpreted as a measurement of the evolution of $\alpha^{-1}(Q^2)$ in the spacelike region between the momentum transfer scales relevant for the analyses. In the small-angle Bhabha scattering analysis these are taken to be the lowest and highest Q^2 values accessible, -2.1 GeV^2 and -6.25 GeV^2 . The difference is found to be

$$\begin{aligned} \alpha^{-1}(-2.1 \text{ GeV}^2) - \alpha^{-1}(-6.25 \text{ GeV}^2) \\ = 0.78 \pm 0.26, \end{aligned}$$

where the error reflects the total experimental uncertainty.

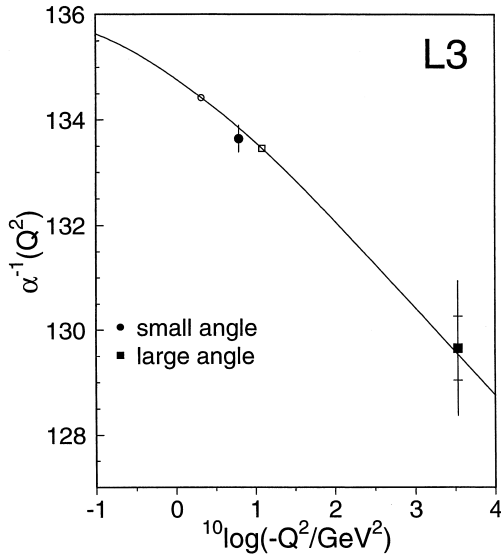


Fig. 3. Measurements of $\alpha^{-1}(Q^2)$ for $Q^2 < 0$. The results of the small-angle and large-angle Bhabha scattering measurements described in this article are shown as a solid circle and square, respectively. The corresponding reference Q^2 values at which the value of $\alpha^{-1}(Q^2)$ is fixed to its expectation are shown as open symbols. The error bar on the large-angle point indicates the experimental and the total uncertainty.

In the large-angle Bhabha scattering analysis the relevant momentum transfer scales are taken to be the average Q^2 value used for the luminosity measurement, -12.25 GeV^2 , and the average Q^2 value for the t -channel contribution to the large-angle Bhabha scattering cross section, -3434 GeV^2 . The result is

$$\alpha^{-1}(-12.25 \text{ GeV}^2) - \alpha^{-1}(-3434 \text{ GeV}^2) = 3.80 \pm 0.61(\text{expt.}) \pm 1.14(\text{theory}).$$

The results are displayed in Fig. 3. For the purpose of the figure, for both measurements the value of $\alpha(Q^2)$ is fixed to its expectation at the lower momentum scale involved in the analysis.

In conclusion, Bhabha scattering at LEP has been used to study the running of the fine-structure constant, $\alpha(Q^2)$, in the spacelike momentum transfer regions $2.1 \text{ GeV}^2 < -Q^2 < 6.25 \text{ GeV}^2$ and $12.25 \text{ GeV}^2 < -Q^2 < 3434 \text{ GeV}^2$. The data clearly establish a nonzero running as predicted by QED.

Acknowledgements

We are grateful for useful discussions with F. Jegerlehner. We wish to express our gratitude to the CERN accelerator divisions for the excellent performance of the LEP machine. We acknowledge the contributions of the engineers and technicians who have participated in the construction and maintenance of this experiment.

References

- [1] S. Tomonaga, Prog. Theor. Phys. 1 (1946) 27; J. Schwinger, Phys. Rev. 74 (1948) 1439; R.P. Feynman, Phys. Rev. 76 (1949) 749; Phys. Rev. 76 (1949) 769.
- [2] CODATA Task Group, to be published in J. Phys. Chem. Reference Data 28, No. 6, 1999; the results can also be found on WWW at <http://physics.nist.gov/constants>.
- [3] E.C.G. Stückelberg, A. Petermann, Helv. Phys. Acta 26 (1953) 499; M. Gell-Mann, F. Low, Phys. Rev. 95 (1954) 1300; N.N. Bogoliubov, D.V. Shirkov, Dokl. AN SSSR 103 (1955) 203.
- [4] S. Eidelman, F. Jegerlehner, Z. Phys. C 67 (1995) 585.
- [5] H. Burkhardt, B. Pietrzyk, Phys. Lett. B 356 (1995) 398.
- [6] M. Steinhauser, Phys. Lett. B 429 (1998) 158.
- [7] M.L. Swartz, Phys. Rev. D 53 (1996) 5268.
- [8] A.D. Martin, D. Zeppenfeld, Phys. Lett. B 345 (1994) 558.
- [9] M. Davier, A. Höcker, Phys. Lett. B 419 (1998) 419.
- [10] J.H. Kühn, M. Steinhauser, Phys. Lett. B 437 (1998) 425.
- [11] R. Alemany, M. Davier, A. Höcker, E. Phys. J. C 2 (1998).
- [12] J. Erler, Phys. Rev. D 59 (1999) 054008.
- [13] S. Eidelman, F. Jegerlehner, A.L. Kataev, O. Veretin, Phys. Lett. B 454 (1999) 369.
- [14] TOPAZ Collaboration, I. Levine et al., Phys. Rev. Lett. 78 (1997) 424.
- [15] VENUS Collaboration, S. Odaka et al., Phys. Rev. Lett. 81 (1998) 2428.
- [16] I.C. Brock et al., Nucl. Instr. Meth. A 381 (1996) 236.
- [17] The L3 detector simulation is based on GEANT Version 3.15. R. Brun et al., GEANT 3, CERN-DD/EE/84-1 (Revised), 1987.
- [18] BHLUMI version 4.04 is used. S. Jadach et al., Comp. Phys. Commun. 70 (1992) 305; Phys. Lett. B 353 (1995) 349; Phys. Lett. B 353 (1995) 362; Comp. Phys. Commun. 102 (1997) 229.
- [19] B.F.L. Ward, S. Jadach, M. Melles, S.A. Yost, Phys. Lett. B 450 (1999) 262.
- [20] L3 Collaboration, B. Adeva et al., Nucl. Instr. Meth. A 289 (1990) 35.
- [21] S. Jadach, W. Placzek, B.F.L. Ward, Phys. Lett. B 390 (1997) 298.
- [22] W. Placzek, private communication.